Application of the general theory of disperse deposits formation in an investigation of mechanism of zinc electrodeposition from the alkaline electrolytes

Nebojša D. Nikolić, Predrag M. Živković, Jelena D. Lović, Goran Branković

PII: S1572-6657(16)30718-4
DOI: doi: 10.1016/j.jelechem.2016.12.024
Reference: JEAC 3020

To appear in: *Journal of Electroanalytical Chemistry*

Received date: 11 August 2016
Revised date: 17 November 2016
Accepted date: 12 December 2016

Please cite this article as: Nebojša D. Nikolić, Predrag M. Živković, Jelena D. Lović, Goran Branković , Application of the general theory of disperse deposits formation in an investigation of mechanism of zinc electrodeposition from the alkaline electrolytes. The address for the corresponding author was captured as affiliation for all authors. Please check if appropriate. Jeac(2016), doi: 10.1016/j.jelechem.2016.12.024

Application of the general theory of disperse deposits formation in an investigation of mechanism of zinc electrodeposition from the alkaline electrolytes

Nebojša D. Nikolić[1,*], Predrag M. Živković[2], Jelena D. Lović[1], Goran Branković[3]

[1]ICTM – Department of Electrochemistry, University of Belgrade, Njegoševa 12, Belgrade, Serbia

[2]Faculty of Technology and Metallurgy, University of Belgrade, Karnegijeva 4, Belgrade, Serbia

[3]Institute for Multidisciplinary Research, University of Belgrade, Kneza Višeslava 1a, Belgrade, Serbia

Abstract. In this study, mehanism of electrodeposition of zinc from the alkaline electrolytes has been investigated using the general theory of disperse deposits formation. The exchange current densities in the range 18.4 – 88 mA cm^{-2} were determined using new method based on comparison of experimental and simulated polarization curves, and the excelent agreement with the values found in the literature has been attained. Correlation between the polarization characteristics and morphologies of zinc deposits characterized by the scanning electron microscopic (SEM) technique was established. The spongy-like particles constructed from nano filaments and the large grains or boulders were formed in the zone of the fast increase of the current density with the overpotential before the plateau of the limiting diffusion current density was reached. The shape of dendrites, formed inside the plateau of the limiting diffusion current density and at the higher ones, strongly depended on overpotential of the electrodeposition. Mechanism of formation of all obtained forms was discussed by the consideration of the different rates of growth of surface protrusions in a function of the overpotential of electrodeposition through the analysis of the change of the ratio between the height and the radius of the protrusions. In order to confirm of the proposed mechanism, comparison with polarization and morphological characteristics of the other metals characterized by the different exchange current density values was made and discussed. Although zinc is classified in the group of the normal metals characterized by the high values of the exchange current density, it was found that the

*Corresponding author: Dr N. D. Nikolić; e-mail: nnikolic@tmf.bg.ac.rs; Tel/fax: + 381 11 337 03 89

polarization and morphological characteristics of zinc show certain and strong similarities with those of copper, classifying zinc just at boundary between the normal and intermediate metals, that is confirmed by the estimation of the exchange current density value for zinc.

Keywords: electrodeposition; zinc; mechanism; filaments; dendrite; boulders; scanning electron microscope (SEM).

1. Introduction

Electrodeposition of zinc attracts an attention from both the academic and technological point of view [1]. In the dependence of later application, the wide spectrum of electrolytes including both acid (chloride [2 – 5] and sulphate [6 – 10]) and alkaline [11 – 19] ones uses for the processes of Zn electrodeposition. The acid electrolytes usually use for a protection of steel against corrosion, where zinc deposits behave as sacrificial anodes and offer cathodic protection of steel [2, 5]. On the other hand, the alkaline electrolytes are used in a Zn-air secondary batteries which are a promising candidate for energy storage with many advantages in relation to the other candidates, such as lithium-air batteries, aluminium-air batteries, and magnesium-air batteries [12]. These advantages are related with an abundance of Zn, low toxicity and low cost, as well as by the fact that Zn posses a relatively high specific energy density [12].

Application of Zn in the above mentioned purposes is strongly related with surface morphology of electrodeposited zinc. As one of the most important characteristics of the electrodeposition processes, morphology of metal deposits depends on both nature of metals and conditions of the electrolysis [20]. According to the kinetic parameters, zinc is situated into the group of *normal metals*, together with Pb, Sn, Tl, Cd, Hg, Ag (simple electrolytes) [21]. The basic characteristics of this group of metals are the high values of the exchange current density (j_0 > 1 A dm^{-2}; j_0 is the exchange current density), low melting points and high overpotentials for hydrogen evolution reaction. From parameters of electrolysis, the most important of them affecting surface morphology of Zn are: the kind and composition of electrolytes, the type of cathodic material, a temperature of electrolysis, a stirring of the electrolyte, a regime of electrolysis (potentiostatic and galvanostatic) [6, 11, 22], *etc.* Also, addition of specific

substances, known as additives, to Zn electroplating baths [3, 8, 13, 15, 16, 18, 19], application of periodically changing regimes (pulsating overpotential, pulsating and reversing currents) of electrolysis [2, 23 – 27], as well as a simultaneous application of both of them [5, 25] can also achieve a strong effect on morphology of zinc deposits. The main purpose of the use of additives and application of periodically changing regimes of electrolysis is to obtain smooth and nanocrystalline deposits of better corrosion resistance [2, 3, 5, 25], often bright coatings [28, 29], or simply to suppress dendritic growth in alkaline Zn-air batteries [13, 15, 16].

The typical morphological forms produced by the processes of Zn electrodeposition from the zincate electrolytes are: spongy-like, boulders and dendrites [14, 30, 31]. Aside from these forms, formation of Zn in the form of filaments, layer-like or mossy has been also reported [11, 12]. The spongy-like and mossy deposits are formed at lower current densities, layer-like at middle current densities and boulders and dendrites are formed at the higher current densities [12, 14]. Mechanisms of formation of majority of these forms, such as spongy-like [32, 33] and dendrites [34], have been separately considered without any correlation between them. Also, some of forms like filaments were only indentified in these investigations without a consideration of mechanism of their formation [11, 12]. A such morphological changes arise from ionic transport through diffusion, migration and convection and several models, such as a concentration-cell model [35] and a hydrodynamic model [36, 37], were proposed to explan it. The changes of surface morphology have been investigated by not only the analysis of deposits obtained in different regimes of electrolysis, but also by digital simulation of the influence of various regimes and parameters of electrolysis [38].

The common characteristic of all these investigations is the absence of a correlation of the electrodeposited forms with the polarization characteristics responsible for their formation. The establishment of this correlation is just one of the basic way to obtain the complete insight in mechanism of electrodeposition of any metal, by which formation of all existing forms would be explained in an unique way. It will be the main aim of this investigation, and will be done through the analysis of zinc electrodeposition processes from the alkaline electrolytes using of the general theory of disperse deposits formation.

2. Experimental

Electrodeposition of zinc was performed in an open cell at the room temperature from the following electrolytes:

(a) 0.10 M ZnO + 6.0 M KOH,

(b) 0.20 M ZnO + 6.0 M KOH,

(c) 0.30 M ZnO + 6.0 M KOH, and

(d) 0.40 M ZnO + 6.0 M KOH.

Doubly distilled water and analytical grade chemicals were used for the preparation of the solutions for the electrodeposition of zinc. In the dependence of type of measurements, electrodepositions were performed on vertical cylindrical copper or zinc electrodes. The geometric surface area of copper and zinc electrodes was 0.5024 cm^2. In all experiments, the reference and counter electrodes were of pure zinc. The counter electrode was a zinc foil with 0.80 dm^2 surface area, which was placed close to the cell walls. The reference electrode was a zinc wire, the tip of which was positioned at a distance of about 0.2 cm from the surface of the working electrode. The working electrodes were placed in the centre of cell, at the same location for each experiment.

Chronopotentiometric measurements were performed using Volta Lab (Radiometer Analytical, Lyon, France). For this type of measurements, the working electrode was of zinc.

The morphologies of Zn deposits were examined using a scanning electron microscope – TESCAN Digital Microscopy. For the morphological analysis, Zn was electrodeposited at copper electrodes from 0.40 M ZnO in 6.0 M KOH in the potentiostatic regime of electrolysis at overpotentials of 25, 65, 125, 150, and 225 mV. At all overpotentials, electrodeposition was performed with quantity of the electricity of 4.50 mA h cm^{-2}, as well as larger or smaller quantities from this one as indicated in Figure caption for each microphotography.

Digital simulation was realized using the software MathLab.

3. Results and discussion

3.1. The polarization and kinetic study of zinc electrodeposition processes

The polarization curves for electrodeposition of zinc from 0.10, 0.20, 0.30 and 0.40 M ZnO in 6.0 M KOH are shown in Fig. 1. In all cases, after the short part characterized by the low nucleation rate (0 - 10 mV), the sharp increase in the current density with increasing the overpotential is observed until the the plateau of the limiting diffusion current density was reached. The fast increase of the current density with increasing the overpotential also followed after the inflection point which denoted the end of the plateau of the limiting diffusion current density. The widths of the plateau of the limiting diffusion current density decreased with increasing concentration of ZnO, and the ranges of overpotentials belonging to the plateaus of the limiting diffusion current density, as well as the values of the limiting diffusion current density, j_L for the examined electrolytes are given in Table 1.

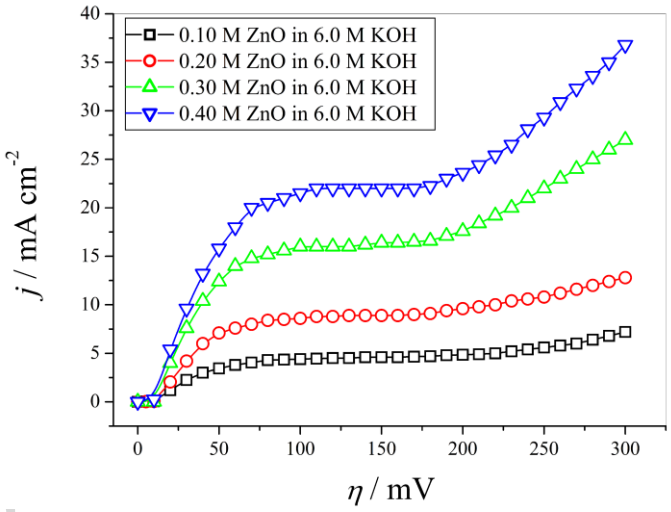

Figure 1. The cathodic polarization curves for electrodeposition of Zn from 0.10, 0.20, 0.30 and 0.40 M ZnO in 6.0 M KOH.

As already mentioned, zinc belongs to the group of *normal metals* characterized by the high values of the exchange current density, the low values of melting point and high values for hydrogen discharge [21]. Since there is no a precise and unique way for determination of the exchange current density of these metals, the exchange current density for zinc was estimated using recently proposed procedure based on a simulation of the polarization curve equation [20,

39]. For those purposes, it is used the polarization curve equation given by Eq. (1), taking the concentration dependence of the exchange current density into account

$$j = \frac{j_0\left(f_c - f_a\right)}{1 + \frac{j_0}{j_L}\left(f_c - f_a\right)} \quad (1)$$

being valid for all j_0 / j_L ratios and overpotentials [20]. In Eq. (1), j is the current density, j_0 is the exchange current density, j_L is the limiting diffusion current density and

$$f_c = 10^{\frac{\eta}{b_c}} \quad \text{and} \quad f_a = 10^{-\frac{\eta}{b_a}}$$

where b_c and b_a are the cathodic and anodic Tafel slopes and η is the overpotential. The Eq. (1) is modified for use in electrodeposition of metals using the values of the cathodic current density and overpotential as positive.

Table 1. The values of the limiting diffusion current density (j_L), the ranges of overpotentials belonging to the plateaus of the limiting diffusion current density ($\Delta\eta$) and the values of exchange current density for electrodeposition of zinc from 0.10, 0.20, 0.30 and 0.40 M ZnO in 6.0 M KOH obtained by comparison of experimental and simulated polarization curves (j_0) and by chronopotentiometry ($j_{0,chrono}$).

Concentration of ZnO, M	j_L, mA cm^{-2}	$\Delta\eta$, mV	j_0, mA cm^{-2}	$j_{0,chrono}$, mA cm^{-2}
0.10	4.6	80 – 180	18.4	4.50
0.20	8.9	90 – 180	35.6	7.12
0.30	16	100 – 180	64	12.7
0.40	22	110 – 180	88	14.8

To enable a digital simulation of the polarization curve equation for the different j_0 / j_L ratios, the Eq. (1) can be re-written in the form:

$$\frac{j}{j_L} = \frac{\frac{j_0}{j_L}(f_c - f_a)}{1 + \frac{j_0}{j_L}(f_c - f_a)} \quad (2)$$

and this form is used for estimation of the exchange current density for zinc.

In the purpose of an estimation of the exchange current density, the polarization curves given in Fig. 1 were standardized to the limiting diffusion current density corresponding to the final value of the current density before the beginning of the sharp increase in the current density after the inflection point. The sharp increase in the current density (the end of the plateau of the limiting diffusion current density) was observed at an overpotential of 180 mV for all electrolytes, and the polarization curves standardized to the current density at this overpotential are shown in Fig. 2a. At the first sight, it can be noticed that there is no any dependence of j / j_L ratios on a concentration of ZnO and for the further analysis, the average values of j / j_L ratios at given overpotential were used. In the next stage, the experimentally obtained average values were compared with the simulated dependencies of $j / j_L - \eta$ obtained for b_a = 40 mV dec^{-1}, b_c = 120 mV dec^{-1} (the values characteristic for zinc [40]) and with j_0 / j_L ratios between 1 and 10, as shown in Fig. 2b. The larger deviation between experimental and simulated values observed at the lower overpotentials can be ascribed to the existence of low nucleation rate in the experimentally recorded polarization curves that cannot be indentified in the simulated polarization curves. Anyway, the good superposition was observed at overpotentials above 80 mV corresponding to the limiting diffusion current density ranges. It is necessary to emphasize that the polarization curves are simulated in a function of j_0 / j_L ratios, and for that reason, the superposition with the experimental curves inside the plateau of the limiting diffusion current density is only relevant for this method of the estimation of j_0. For the sake of precise estimation of the exchange current density values, the enlarged part from Fig. 2b is shown in Fig. 2c. It can be noticed from Fig. 2c that the nearest superposition between the experimental and simulated values was obtained for j_0/j_L = 4. Using this value, as well as the values of the limiting diffusion current density given in Table 1, the exchange current densities were estimated, and the obtained values were included in Table 1. The obtained values between 18.4 – 88 mA cm^{-2} were in the excellent agreement with those proposed by Bockris *et al.* [40] (j_0 between 8 and 370 mA cm^{-2})

for this type of electrolyte, confirming a validity of this procedure for estimation of the exchange current density of the *normal metals*.

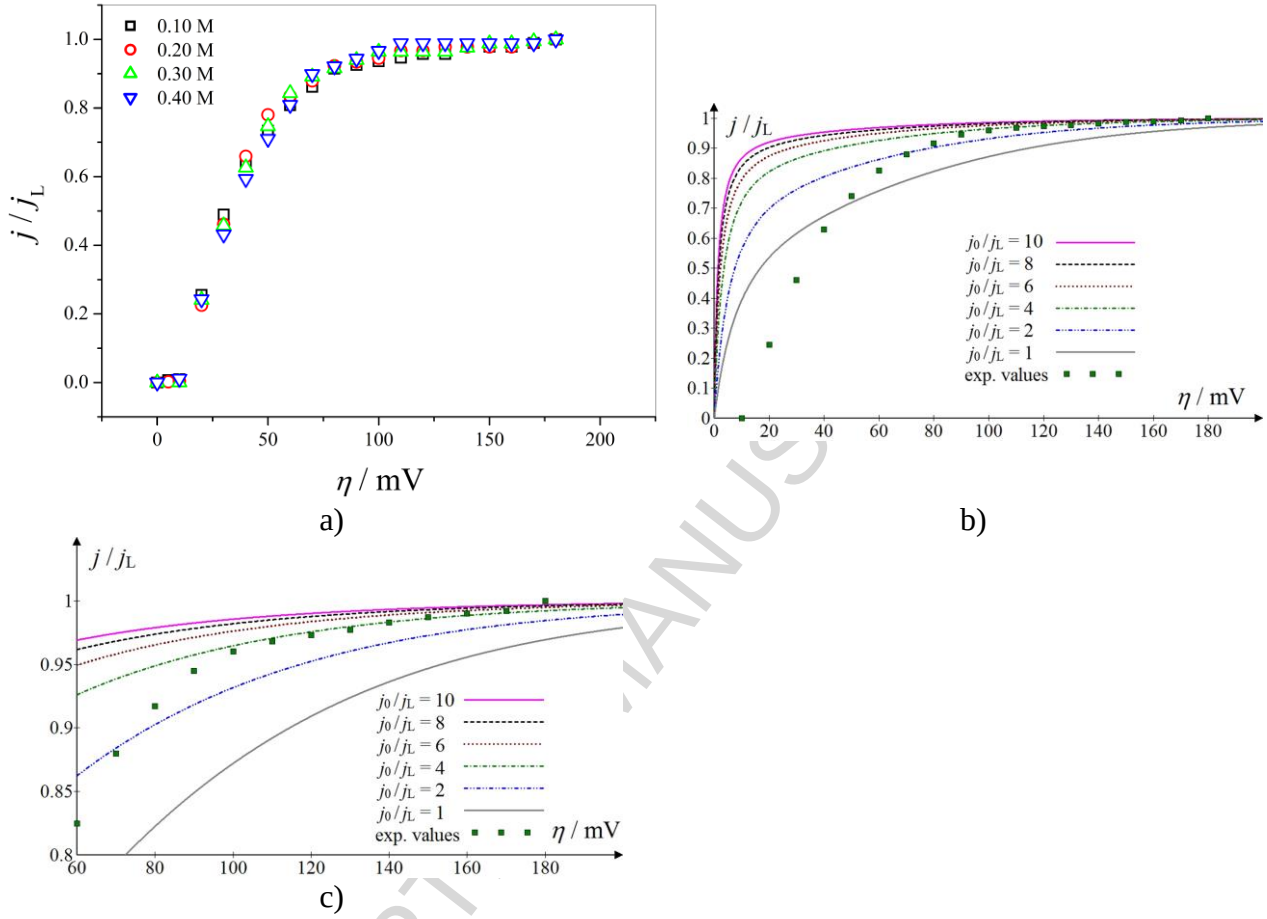

Figure 2. a) The polarization curves for electrodeposition of Zn from 0.10, 0.20, 0.30 and 0.40 M ZnO in 6.0 M KOH standardized to the limiting diffusion current densities, b) comparison of experimental values and simulated dependencies of $j / j_L - \eta$ obtained using Eq. (2) for b_a = 40 mV dec^{-1}, b_c = 120 mV dec^{-1} and j_0 / j_L ratios between 1 and 10, and c) the enlarged part from Fig. 2b.

The obtained values are compared with those obtained by chronopotentiometric method following procedure given in Ref. [10]. In chronopotentiometry, the overpotential dependence on time is given by Eq. (3) [10, 41]:

$$\eta = -\frac{RT}{\alpha n F}\ln\frac{j}{j_0} + \frac{RT}{\alpha n F}\ln\left(1-\sqrt{\frac{t}{\tau}}\right) \qquad (3)$$

where are: R is the universal gas constant, T is the temperature, α is the charge transfer, n is the number of electrons, F is the Faraday constant, t is the time, and τ is the transition time.

Figure 3a and b shows chronopotentiograms obtained from all four electrolytes at current densities which were twice larger than the corresponding limiting diffusion current density (Fig. 3a) and the dependencies $\eta - \ln\left(1-\sqrt{\frac{t}{\tau}}\right)$ derived from the chronopotentiograms by the application of Eq. (3) (Fig. 3b). The way of determination of the transition time is shown in Fig. 3a, while the exchange current densities were determined from the segment at the overpotential axis (Fig. 3b). The exchange current densities obtained in this way ($j_{0,\mathrm{chrono}}$) are also given in Table 1.

At the first sight, it can be noticed that although the obtained values were smaller than those obtained by comparison of experimental and simulated curves and those found in Ref. [40], they were of the same order of magnitude. This difference decreases with increasing the current density of electrodeposition, as seen by the analysis of Fig. 3c and d showing chronopotentiograms and the corresponding $\eta - \ln(1-\sqrt{t/\tau})$ dependencies obtained with ZnO concentration of 0.10 M at current densities which corresponded to twice (j = 9.2 mA cm^{-2}), 2.5 times (j = 11.5 mA cm^{-2}) and 3.5 times (j = 16.1 mA cm^{-2}) larger values than the limiting diffusion current density. From Fig. 3d, it can be noticed that the segments for η = 0 and the slopes of $\eta - \ln(1-\sqrt{t/\tau})$ dependencies did not depend on the current density of electrodepostion. The obtained j_0 values were: 4.50 mA cm^{-2} (at 9.2 mA cm^{-2}), 5.35 mA cm^{-2} (at 11.5 mA cm^{-2}), and 7.0 mA cm^{-2} (at 16.1 mA cm^{-2}).

The obtained differences in the j_0 values can be ascribed by the different diagnostic criteria on which these two ways for the estimation of the exchange current density are based. Namely, the chronopotentiometric method is based on the charge transfer, while the new method proposed in this investigation takes into consideration the limiting diffusion current density as diagnostic criteria. However, how zinc belongs to the group of *normal metals* characterized with the fast charge transfer, the values obtained by chronopotentiometric method can be also observed as the relative values, not absolutely ones. The advantage of the way proposed here lies in the possibility of estimation of the exchange current density of all metals with fast charge

transfer including those like Pb with the extremely fast charge transfer, where the chronopotentiometric method is inapplicable. Also, unlike from chronopotentiometry the method based on the comparison of experimental and simulated polarization curve does not depend on the current density of electrodeposition.

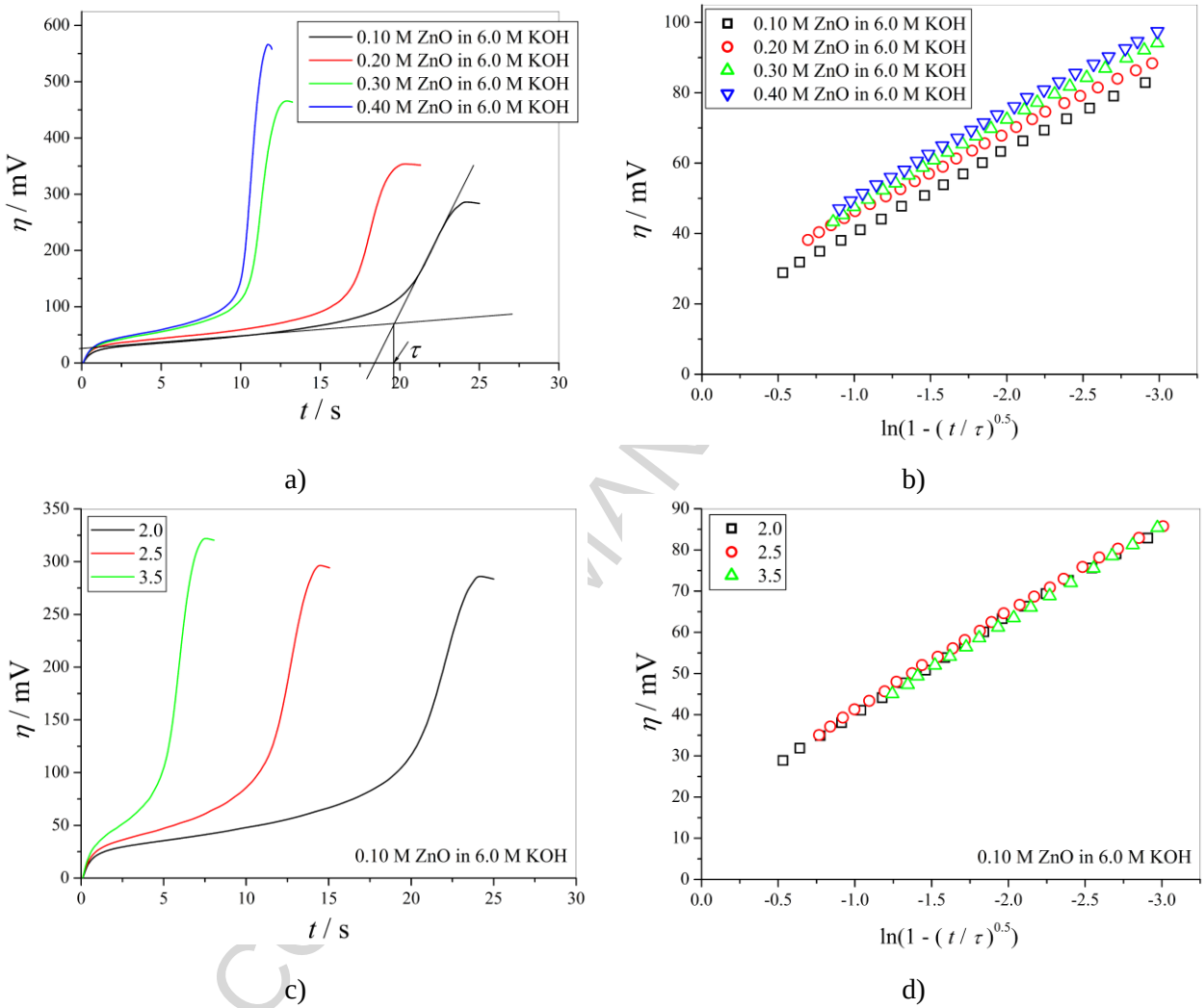

Figure 3. a) Chronopotentiograms obtained at twice larger current densities than the limiting diffusion current densities: a) 9.2 mA cm^{-2} (for 0.10 M ZnO), 17.8 mA cm^{-2} (for 0.20 M ZnO), 32 mA cm^{-2} (for 0.30 M ZnO) and 44 mA cm^{-2} (for 0.40 M ZnO), and b) the dependencies $\eta - \ln(1-\sqrt{t/\tau})$ for the same electrolytes. In all cases: 6.0 M KOH, c) Chronopotentiograms obtained from 0.10 M ZnO in 6.0 M KOH at twice (9.2 mA cm^{-2}), 2.5 (11.5 mA cm^{-2}) and 3.5 (16.1 mA cm^{-2}) times larger current densities than the limiting diffusion current density, and d) the corresponding $\eta - \ln(1-\sqrt{t/\tau})$ dependencies.

3.2 Morphological study of zinc electrodeposition processes from 0.40 M ZnO in 6.0 M KOH

The different positions at the polarization curve recorded from 0.40 M ZnO in 6.0 M KOH were characterized by the scanning electron microscopic (SEM) analysis of electrodeposited zinc and the obtained surface morphologies are shown in Figs. 4 and 5 (the range of overpotentials up to a reaching of the plateau of the limiting diffusion current density), Figs. 6 and 7 (the plateau of the limiting diffusion current density) and Fig. 8 (the zone of the fast increase in the current density with the increase of overpotential after the inflection point).

The deposit constructed from the spongy-like particles, also often referred as a mossy one, is formed at an overpotential of 25 mV (Fig. 4). The ratio of the initial current density of electrodeposition to the limiting diffusion current density leading to formation of these particles was approximately 0.30 ($j / j_L \approx 0.3$). The spongy-like particles were approximately the same size indicating on their simultaneously formation (Fig. 4a and b). The prolonging electrodeposition time leads to growth of the spongy-like particles in all directions causing a joining of neighboring particles (Fig. 4c – g). Analysis of the spongy-like particles at the higher magnifications revelas that these particles are constructed from intertwined nano size filaments (Fig. 4h and i).

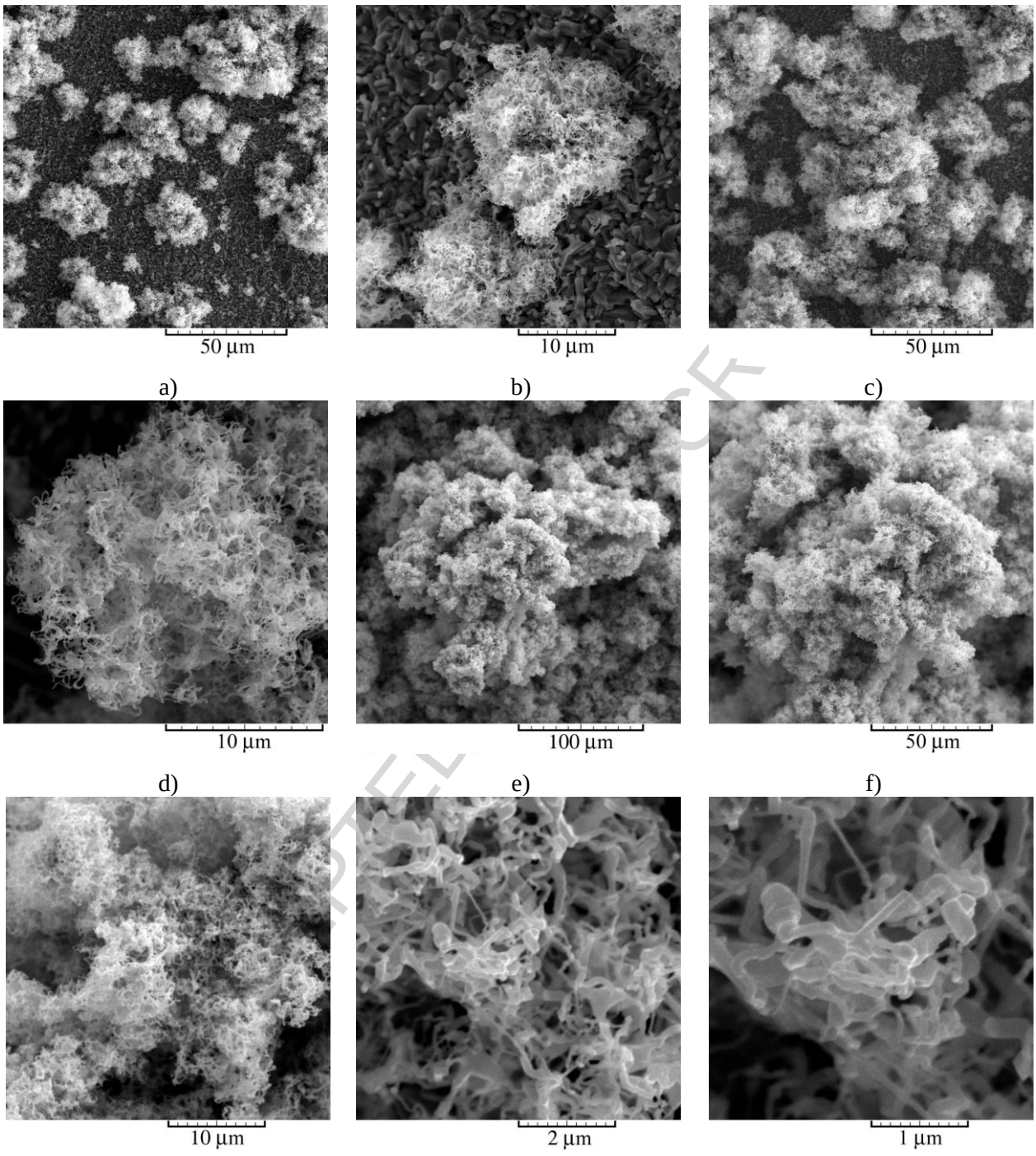

Figure 4. The spongy-like particles obtained by electrodeposition from 0.40 M ZnO in 6.0 M KOH at an overpotential of 25 mV with a quantity of the electricity of: a) and b) 1.6 mA h cm^{-2}, c) and d) 2.4 mA h cm^{-2}, e) , f) and g) 4.5 mA h cm^{-2}, h) and i) The filaments of which the spongy-like structure is constructed.

The spongy-like growth has been terminated at about $j / j_L \approx 0.5$, and the completely different situation was observed at an overpotential of 65 mV at which the ratio of the initial current density to the limiting diffusion current density was approximately 0.9 ($j / j_L \approx 0.9$). The layer-structure is predominantly formed with the smaller quantity of passed electricity (Fig. 5a – c) and large grains, often reffered as boulders, were formed with the larger quantity of passed electricity (Fig. 5d – f) at an overpotential of 65 mV.

Figures 6 and 7 show the zinc deposits obtained at overpotentials of 125 mV (Fig. 6) and 150 mV (Fig. 7) belonging to the plateau of the limiting diffusion current density. From Fig. 6, it can be seen that dendritic growth is already initiated at an overpotential of 125 mV (Fig. 6a and b), and that the further growth primarily occurs on dendrites due to the current density distribution effect [20], as seen from Fig. 6c and d showing zinc dendrites obtained with the larger quantity of electricity. The shape of dendrites changed with increasing overpotential, as shown in Fig. 7. It is necessary to note that numerous crystals with well defined crystal planes are formed among the dendritic particles.

The very branchy dendrites of zinc were formed at an overpotential of 225 mV in the zone of fast increase of the current density with increasing overpotential (Fig. 8a and b). Aside from the dendrites as the dominant morphological form, the position at the electrode surface created as a consequence of hydrogen evolution as the second reaction to Zn electrodeposition can be also noticed in the zinc deposit electrodeposited at this overpotential (Fig. 8c and d). With the increasing quantity of the electricity (Fig. 8e), the electrodeposition process occurs primarily through the further growth of dendrites.

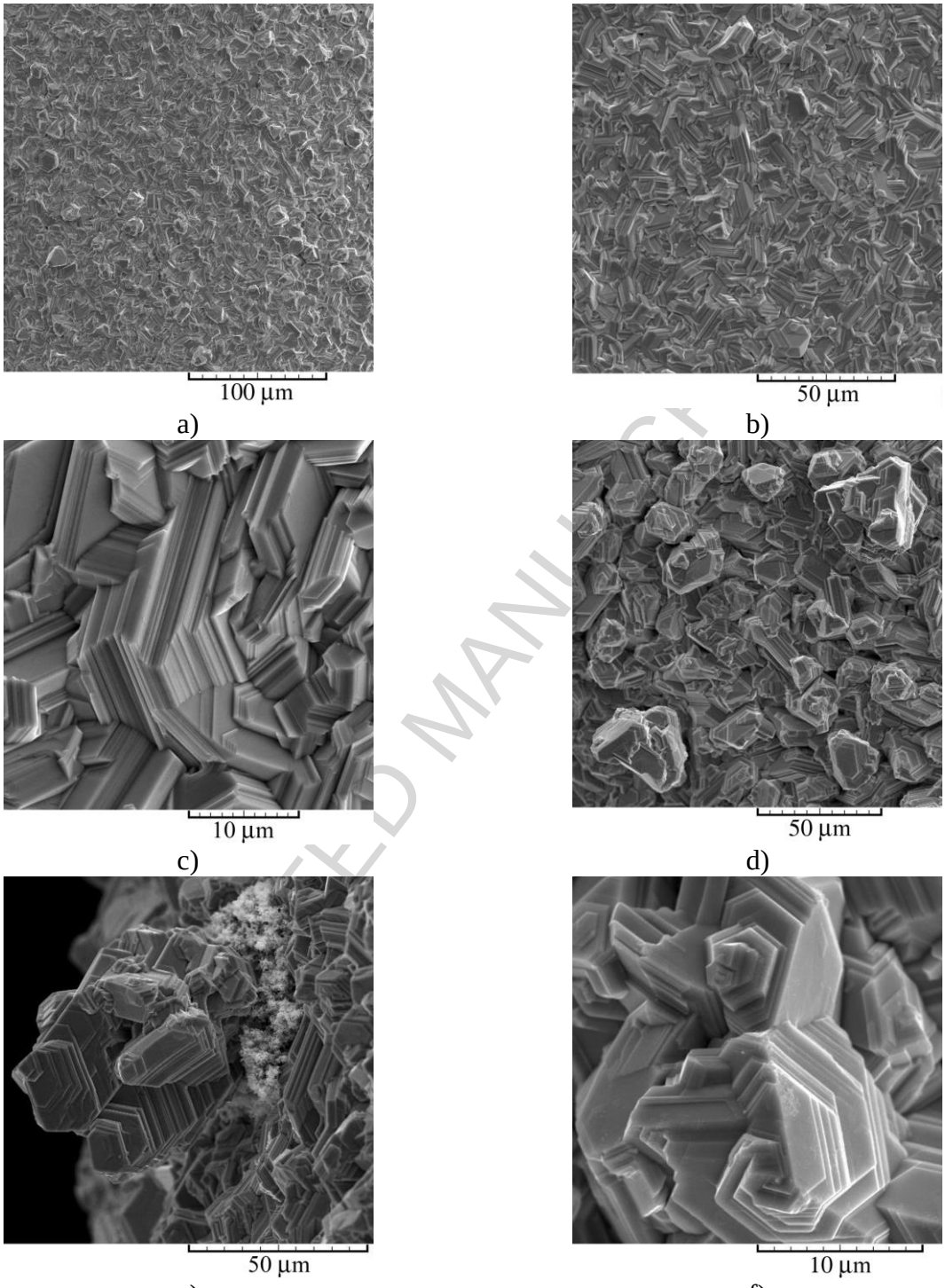

Figure 5. The Zn deposits obtained by electrodeposition from 0.40 M ZnO in 6.0 M KOH at an overpotential of 65 mV with a quantity of the electricity of: a), b) and c) 4.5 mA h cm^{-2}, d), e) and f) 12.0 mA h cm^{-2}.

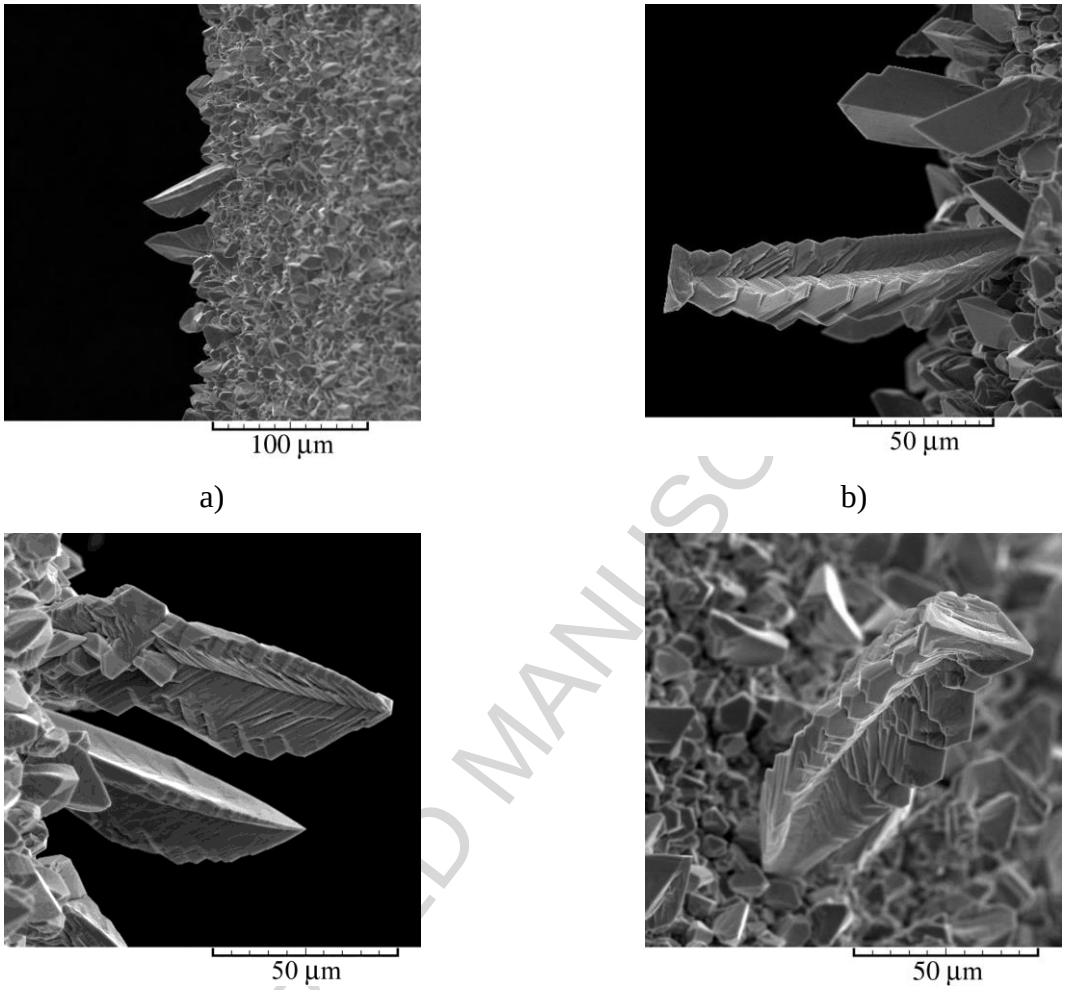

Figure 6. The dendrites of Zn electrodeposited from 0.40 M ZnO in 6.0 M KOH inside the plateau of the limiting diffusion current density at an overpotential of 125 mV: a) and b) the quantity of electricity: 4.5 mA h cm^{-2}; c) and d) the quantity of electricity: 6.75 mA h cm^{-2}.

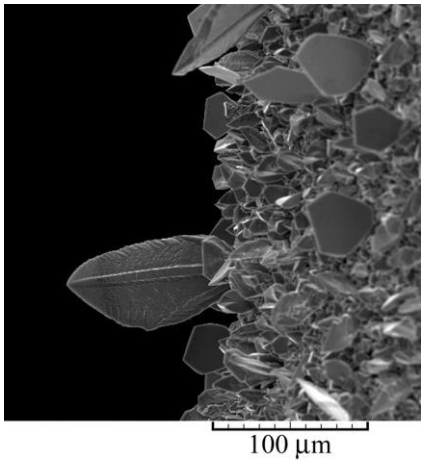

a)

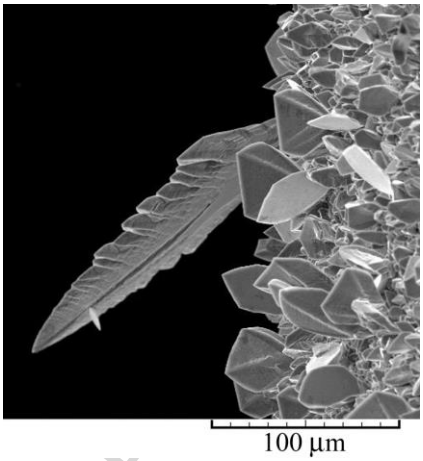

b)

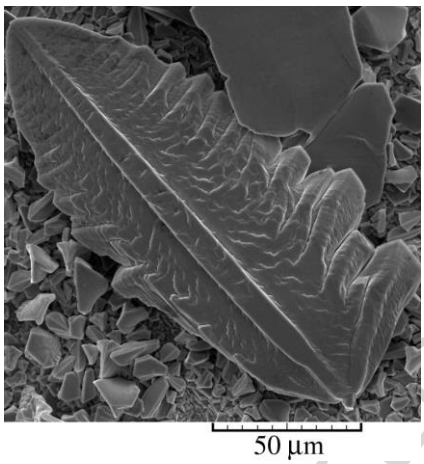

c)

Figure 7. The dendrites of Zn electrodeposited from 0.40 M ZnO in 6.0 M KOH inside the plateau of the limiting diffusion current density at an overpotential of 150 mV; the quantity of electricity: 4.50 mA h cm^{-2}.

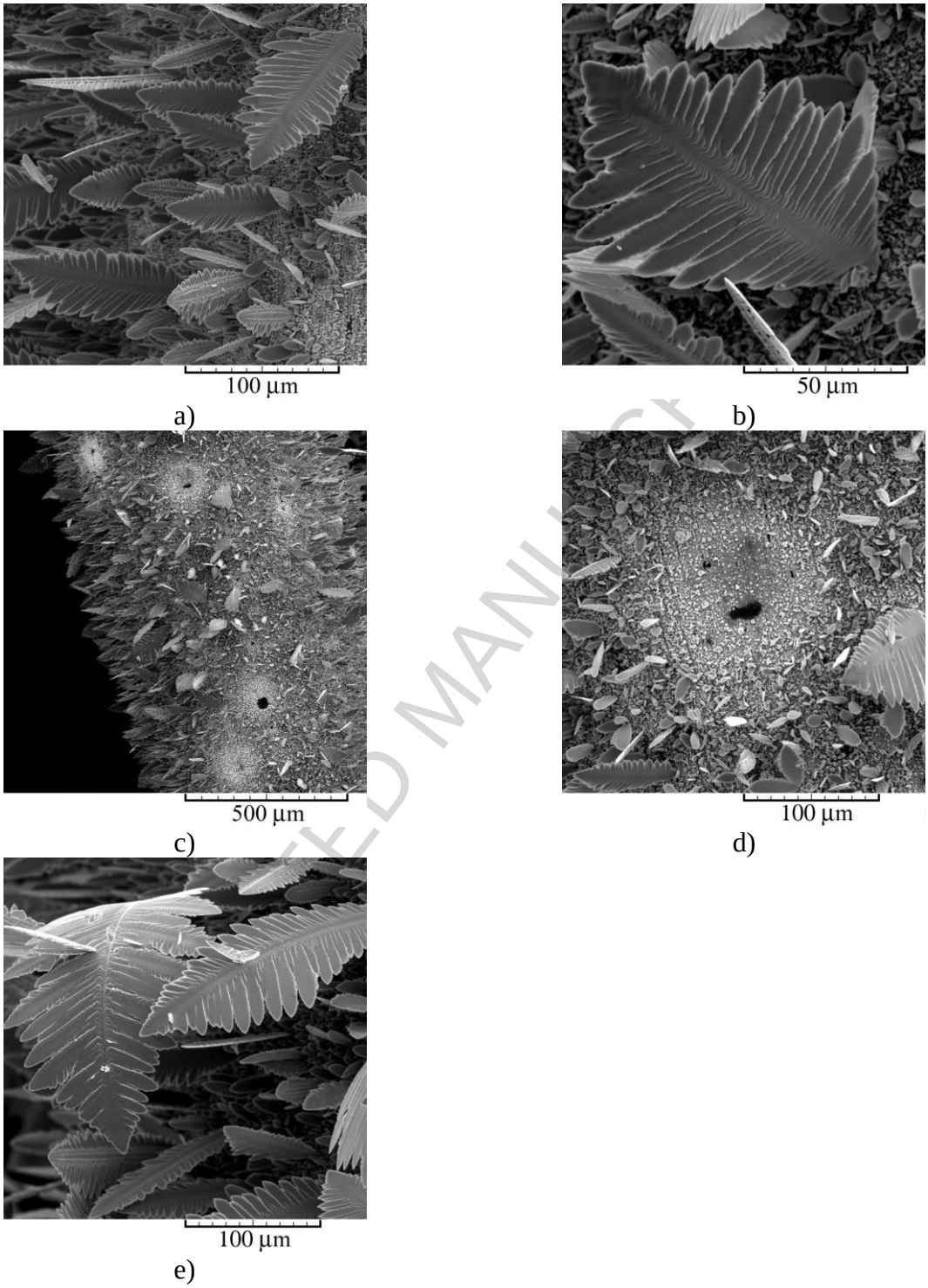

Figure 8. Morphologies of Zn deposits electrodeposited from 0.40 M ZnO in 6.0 M KOH at an overpotential of 225 mV (outside the plateau of the limiting diffusion current density): a) and b) dendrites, c) and d) hydrogen evolution effect. The quantity of passed electricity: 2.25 mA h cm^{-2}; e) dendrite obtained with a quantity of electricity of 4.5 mA h cm^{-2}.

3.3. Discussion of the presented results

The dependence of the logarithm of the limiting diffusion current density on the logarithm of concentration of ZnO is shown in Fig. 9. The linear dependence with a slope of 1.21 was obtained. On the basis of this value, it is clear that electrodeposition of Zn occurs in the conditions of natural convection because the obtained value was very close to the theoretical value for this type of convection predicted by Levich [42]. Namely, according to Levich [42], if electrodeposition process occurs in the conditions of natural convection, the limiting diffusion current density, j_L depends on concentration of depositing ions, c as $j_L \sim c^{1.25}$. This dependence is valid under proper isothermal conditions, when the temperatures of the thermostated solutions (with a free surface) and of surrounding air are equal. It is necessary to note that the similar dependencies were obtained in the case of Pb [43] and Cu [44], confirming this type of convection in the case of Zn electrodeposition from this type of electrolyte.

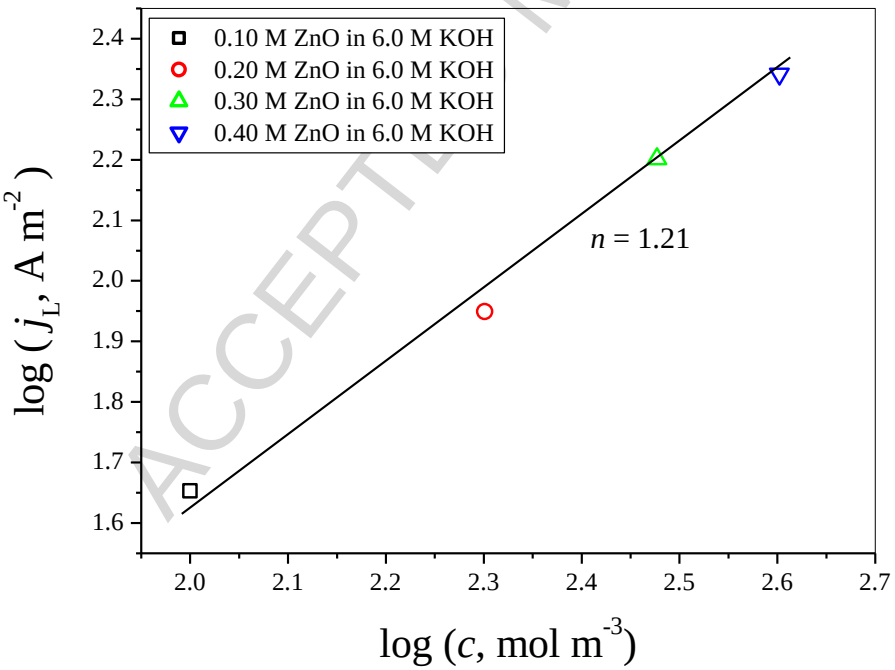

Figure 9. The logarithmic dependence of the limiting diffusion current density, j_L on the concentration of solution, c.

Although Zn belongs to the group of *normal metals*, the shape of the polarization curves shown in Fig. 1 shows certain similarities to those for copper and the silver (complex ammonium electrolyte) belonging to the group of *intermediate metals* (for the group of *intermediate metals* it is valid lower values of both the exchange current densitiy; $10^{-2} < j_0 < 1$ A dm^{-2} and hydrogen evolution overpotentials than those for the *normal metals* [21]). In the case of Zn, the linear dependences of the current density on the overpotential (the ohmic control) observed in the initial parts of the polarization curves for Ag [45] and Pb [43], as the typical representatives of the group of *normal metals*, are not observed regardless of concentration of ZnO. Comparing the polarization characteristics of the *normal* and *intermediate metals*, it is clear that zinc is "slower" metal than lead [43] or the basic electrolytes of silver [45], but it is "faster" than copper [44] and the ammonium electrolyte of silver [46]. For example, in the case of copper and silver, the widths of the plateau of the limiting diffusion current density are between 300 and 750 mV (0.10 M $CuSO_4$ in 0.50 M H_2SO_4), and between 250 and 700 mV (0.10 M $AgNO_3$ in 0.50 M $(NH_4)_2SO_4$ solution to which was added ammonium hydroxide to dissolve the silver sulphate precipitate) [46]. On the other hand, the plateaus of the limiting diffusion current density are not observed or were very short in the case of electrodeposition of the *normal metals*. For example, the inflection point is usually observed in the case of lead at an overpotential of 55 mV [43, 47]. Furthermore, the estimated values of the exchange current density for zinc ($j_0 > 1.84$ A dm^{-2}) were very close to the lower limit for *the normal metals* ($j_0 > 1$ A dm^{-2}), classifying Zn in regard to kinetic parameters at the boundary between the *normal* and *intermediate metals*. These characteristics of Zn just enabled to make analogy between the electrodeposition processes of Zn and metals from the group of the *intermediate ones*, with the aim to obtain a comprehensive insight into mechanism of Zn electrodeposition by using the general theory of disperse deposits formation.

3.3.1. The basis of the general theory of disperse deposits formation and its application in understanding of morphological changes of Zn

The limiting diffusion current density to the tip of any protrusion schematic presented in Fig. 10a, $j_{L,tip}$ is given by Eq. (4) [20, 48]:

$$j_{\mathrm{L,tip}} = j_{\mathrm{L}}\left(1+\frac{2h^2}{R^2}\right) \tag{4}$$

where j_{L} is the limiting diffusion current density to the flat electrode surface, h is the height of protrusion, and R is the radius of the protrusion base, or

$$j_{\mathrm{L,tip}} = j_{\mathrm{L}}(1+2k^2) \tag{5}$$

since

$$k = \frac{h}{R} \tag{6}$$

The current density to the tip of such protrusion, j_{tip} is given by Eq. (7) [20, 48]:

$$j_{\mathrm{tip}} = \frac{j_0(f_{\mathrm{c}} - f_{\mathrm{a}})}{1+\frac{j_0}{j_{\mathrm{L}}}\cdot\frac{1}{1+2k^2}f_{\mathrm{c}}} \tag{7}$$

taking the cathodic current density and overpotential to be positive.

As already mentioned, the spongy-like particles are formed at the low overpotentials in the initial part of the polarization curve characterized by the fast increase in the current density with the overpotential up to about $j / j_{\mathrm{L}} \approx 0.5$. The spongy-like particles are constructed from very fine filaments (Fig. 4h and i) and formation of this filamentary structure can be considered as follows: it can be assumed that electrodeposition process in the initial stage at the low overpotentials commences by formation of small number of hemispherical nuclei. These nuclei grow under the activation control because a pure activation control is even possible in systems for which $j_0 >> j_{\mathrm{L}}$ is valid on very small electrodes, like nuclei on an inert electrode [20].

For hemispherical nuclei (Fig. 10a), $h_{\mathrm{s}} = R$, and the limiting diffusion current density to the tip of nuclei is given according to Eqs. (5) and (6) by Eq. (8):

$$j_{\mathrm{L,tip}} = 3j_{\mathrm{L}} \tag{8}$$

that can be applied for every protrusion at the electrode surface, and hence, for hemispherical nuclei. Then, according to Eq. (7) the current density on the tip of hemispherical protrusion becomes somewhat larger than the current density to the flat part of the electrode surface. The

larger current density on the tips of hemispherical nuclei leads to their enhanced growth and transformation into parabolic protrusion (Fig. 10a). The tip radius of the parabolic protrusion is

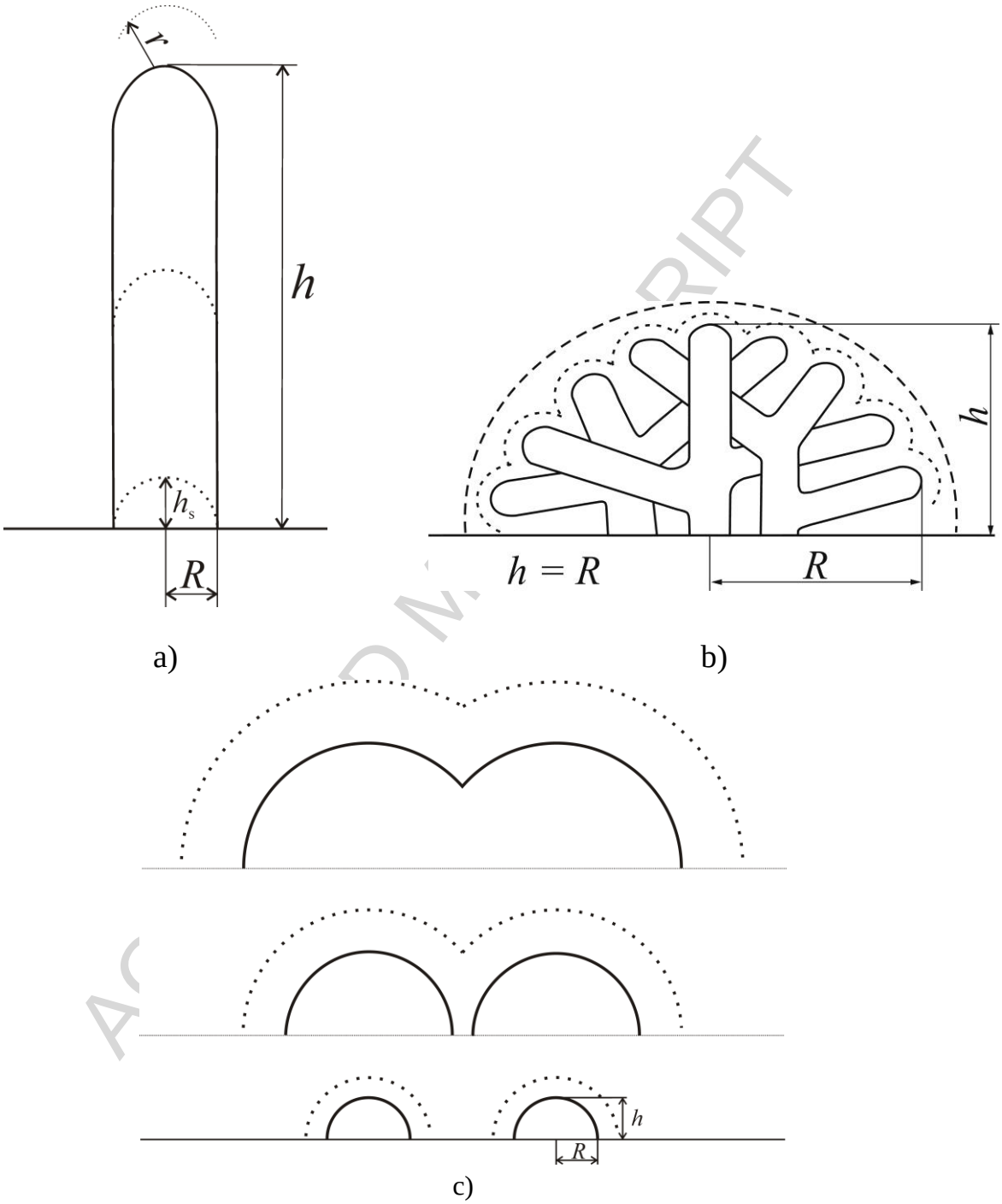

Figure 10. Shematic presentations of formation of: a) filament and b) the spongy-like particle, and c) overlap of neighbor spongy-like particles.

determined by Eq. (9) [20, 48]:

$$r = \frac{R^2}{2h}, \tag{9}$$

and the local spherical diffusion layers of the same radius are formed around the tips of such protrusions. The further growth occurs inside these spherical diffusion fields leading to Zn electrodeposition in the form of filaments. In the process of growth of filaments, due to very small radius of hemispherical nuclei, the condition $h >> R$ is very fast fulfilled, and the growth of filaments occurs under the activation control relative to the surrounding electrolyte, but under the mixed activation-diffusion control in the relation to the flat part of the electrode surface. With the electrodeposition time, due to the new nucleation, lateral growth also takes place causing branching of the filaments. Simultaneously, the neighbor branchy filaments mutually interweave giving to particles the spongy-like appearance.

The spherical diffusion layers are formed around so obtained the spongy-like particles, as schematically presented in Fig. 10b. With the increase of the amount of passed electricity (Fig. 4c and d), the neighbor spongy-like particles mutually merge and a coverage of the electrode surface by them increases. Finally, a full coverage of the electrode surfaces by the spongy-like particles is expected for the long electrodeposition times (Fig. 4e and f). Simultaneously, the spherical diffusion layers formed around the spongy-like particles mutually overlap causing that the further growth occurs in the diffusion layer of the macroelectrode (Fig. 10c). It is very clear that since the growth of the spongy-like particle occurs simultaneously in all directions at the approximately same rate, the condition $h \approx R$ is valid for this type of particle, where h is the height and R is the radius of the spongy-like particle.

From the above consideration, it is clear that the spongy-like particles are formed at the low overpotentials in the conditions of slow nucleation. With the increasing overpotential of electrodeposition, the nucleation and deposition rate increase leading to inhibition of the spongy-like growth. At the higher overpotentials close to the plateau of the limiting diffusion current density, the large grains, often referred as boulders, are obtained (Fig. 5). The shape of these grains, as well as their formation close to the plateau of the limiting diffusion current density, clearly indicates that there is a similarity with formation of cauliflower-like particles during Cu

electrodeposition [20]. In this way, mechanism of Zn electrodeposition will additionally approach to mechanism of electrodeposition of the *intermediate metals*.

Then, formation of the large grains or boulders shown in Fig. 5 can be considered as follows: analysis of these grains at the higher magnification (Fig. 5e and f) revealed that they are formed by the pyramid-like growth, as proposed by Diggle *et al.* [34] for the dendritic growth. The similar to parabolic protrusion, the spherical diffusion layers are formed around the tips of pyramid-like protrusions as illustrated in Fig. 11. In the initial stage of electrodeposition, the height of a protrusion is small, $h \to 0$, and then, $r \to \infty$ since $R \neq 0$. The spherical diffusion layer cannot be formed around such protrusion and the growth process occurs in the conditions of linear diffusion control following mechanism of non-dendritic amplification of surface coarseness (Fig. 5a – c) [20]. The height of pyramid-like protrusions increases with a quantity of passed electricity ($h > R$) and then, the spherical diffusion layers can be established around the tips of such protrusions causing the decrease of the radius of the tip in accordance with Eq. (9). If pyramid-like protrusion is sufficiently far from the other ones, the spherical diffusion layer can be formed around the whole protrusion enabling the growth of second generation of protrusions inside the diffusion layer of the initially formed protrusion, as seen in Fig. 5e. In this way, a similarity with formation of cauliflower-like particles of copper is proved [20].

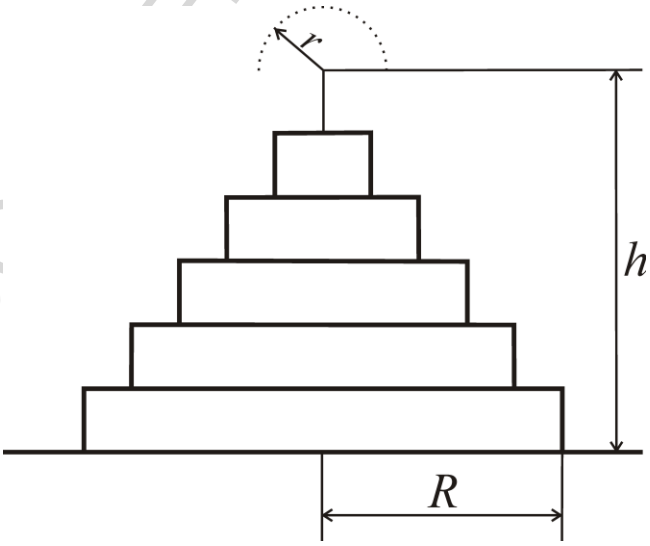

Figure 11. Shematic presentation of pyramid-like growth.

This established similarity with copper electrodeposition processes also persists during electrodeposition inside the plateau of the limiting diffusion current density and at the higher ones. The dendritic growth has been already initiated at an overpotential of 125 mV belonging to the plateau of the limiting diffusion current density (Fig. 6). The critical overpotential for initiation of dendritic growth, η_i can be presented by Eq. (10) [20, 48]:

$$\eta_i = \frac{b_c}{2.3} \ln \frac{j_L}{j_0} \qquad (10)$$

From Fig. 6b and d, it is necessary to note that some of the formed dendrites have not the tip as one of the basic characteristics of dendritic growth, but they show well defined plane which indicates that the growth occurs predominately in the conditions of cylindrical diffusion [47]. The increasing overpotential inside the plateau of the limiting diffusion current density leads to formation of dendrites in accordance with Wranglen's definition of dendrites. According to Wranglen [49], a dendrite is a skeleton of a monocrystal and consists of a stalk and branches, thereby resembling a tree. The dendrite consisted only of the stalk and primary branches are referred as primary (P) dendrite. If the primary branches in turn develop secondary branches, the dendrite is called secondary (S). The two-dimensional (2D) dendrite refers to dendrites with branches that lie in the same plane as that of the primary stalk [49].

Zinc dendrites with a defined stalk, but without defined branches are formed at an overpotential of 150 mV (Fig. 7). The futher increase in overpotential of the electrodeposition outside the plateau of the limiting diffusion current density leads to formation of more branchy dendrites. Namely, the dendrites with well defined stalk and primary branches are formed at an overpotential of 225 mV in the zone of the fast increase of the current density with increasing overpotential after the inflection point (Fig. 8a, b and e). The critical overpotential for the instantaneous dendritic growth, η_c is defined by the end of the plateau of the limiting diffusion current density (the inflection point) and given by Eq. (11) [20, 48]:

$$\eta_c = \frac{b_c}{2.3} \ln \left[\frac{j_L}{j_0} \left(\frac{\delta}{h} \right)^{\gamma} \right] \qquad (10)$$

where δ is the diffusion layer thickness and $\gamma = \frac{\mathrm{d} \log j_0}{\mathrm{d} \log c}$ [50].

In this case, $h >> R$, $k \rightarrow \infty$ (Eq. (6)), and according to Eq. (5), $j_{L,tip} \rightarrow \infty$. The current density on the tip of a protrusion (Eq. (7)) transforms into the form $j_{tip} \rightarrow j_0 (f_c - f_a) >> j$. This means that the tip of a dendrite protrusion grows under pure activation control outside the diffusion layer of the macroelectrode. Inside it, it grows under the activation control relative to the surrounding electrolyte, but under mixed activation-diffusion control relative to the bulk electrolyte [20, 34, 51]. Hence, the fast increase of the current density with increasing overpotential after the inflection point can be ascribed to the activation control at the tips of dendrites in accordance with Diggle, Despić, Bockris theory [34], where the tips of dendrites grow under the activation control while electrodeposition on the macroelectrode is simultaneously diffusion controlled process. It is necessary to note that the tips of both stalk and branches contribute to this fast growth of the current density after the inflection point.

Aside from the well defined dendrites, holes which origin is of detached hydrogen bubbles are also formed by electrodeposition of Zn at 225 mV (Fig. 8c and d). The number of formed holes was relatively small, and formation of well defined dendrites around the position at which hydrogen evolution is commenced clearly indicates that evolution of hydrogen was insufficient that achieve any influence on the hydrodynamic conditions in the near-electrode layer. In this way, the growth of the current density after the inflection point was only due to the activation control at the tips of dendrites.

4. Conclusion

The processes of electrodeposition of zinc from the alkaline electrolytes have been investigated by the analysis of the polarization characteristics and the scanning electron microscopic (SEM) analysis of deposits obtained in the potentiostatic regime of electrolysis. The exchange current densities for the processes of Zn electrodeposition estimated in the interval between 18.4 and 88 mA cm^{-2} by comparison of the experimental and simulated polarization curves were in a line with those found in the literature, and larger than those determined by chronopotentiometry. Using the general theory of disperse deposits formation, mechanism of formation of specific disperse forms, such as spongy-like, large grains (boulders) and dendrites of various shape, was explained. All these surface morphologies were formed from protrusions or

irregularies at the electrode surface characterized by a height (h) and the radius of base (R). The final morphology of electrodeposited Zn is determined by the different rates of growth in a function of overpotential of the electrodeposition, and hence, by the ratio between the height and radius of protrusion.

The spongy-like particles are constructed from filaments at the nano level and the growth of filaments commences from a hemispherical nuclei for which $h_s = R$. In the growth process, due to the larger current density at the tip of nuclei, h_s becomes larger than R and their transformation in a protrusion like filament takes place. For the spongy-like particles, the condition $h \approx R$ is valid, where h is the height of the whole spongy-like particle.

The large grains or boulders are formed by the pyramid-like or by the growth at the screw dislocation in the conditions of non-dendritic amplification of surface protrusions for which $h > R$ is valid. The both spongy-like particles and boulders were formed at the overpotentials before a reaching of the plateaus of the limiting diffusion current density.

The dendrites are formed at overpotentials belonging to the plateau of the limiting diffusion current density and at the higer ones. The shape and ramification of dendrites increased with increasing the overpotential of electrodeposition. In the case of dendritic growth, the condition $h >> R$ is fulfilled, and the tips of dendrites grow under the activation control, while the growth at the flat part of electrode surface is diffusion controlled process.

From point of view of polarization and morphological characteristics, it is concluded that mechanism of Zn electrodeposition is more similar to a mechanism of electrodeposition of *intermediate metals* (Cu, the complex electrolytes of Ag, Au) than to mechanism characterizing electrodeposition of the other *normal metals* like Pb and Ag (the simple electrolytes).

Acknowledgement: This work was supported by the Ministry of Education, Science and Technological Development of the Republic of Serbia.

References:

[1] R. Winand, Electrodeposition of Zinc and Zinc Alloys, in: M. Schlesinger, M. Paunovic (Eds.,) Modern Electroplating, Fifth Edition John Wiley & Sons, Inc., Hoboken, NJ, 2010, p.p. 285–307.

[2] Kh. M. S. Youssef, C. C. Koch, P. S. Fedkiw, Improved corrosion behavior of nanocrystalline zinc produced by pulse-current electrodeposition, Corros. Sci. 46 (2004) 51–64.

[3] M. Mouanga, L. Ricq, G. Douglade, J. Douglade, P. Bercot, Influence of coumarin on zinc electrodeposition, Surf. Coat. Technol. 201 (2006) 762–767.

[4] P. -C. Hsu, S. -K. Seol, T. -N. Lo, C. -J. Liu, C. -L. Wang, C. -S. Lin, Y. Hwu, C. H. Chen, L. -W. Chang, J. H. Je, G. Margaritondo, Hydrogen Bubbles and the Growth Morphology of Ramified Zinc by Electrodeposition, J. Electrochem. Soc. 155 (2008) D400–D407.

[5] M. Mouanga, L. Ricq, J. Douglade, P. Bercot, Corrosion behaviour of zinc deposits obtained under pulse current electrodeposition: Effects of coumarin as additive, Corros. Sci. 51 (2009) 690–698.

[6] K. Raeissi, A. Saatchi, M. A. Golozar, Effect of nucleation mode on the morphology and texture of electrodeposited zinc, J. Appl. Electrochem. 33 (2003) 635–642.

[7] O. Aaboubi, J. Douglade, X. Abenaqui, R. Boumedmed, J. VonHoff, Influence of tartaric acid on zinc electrodeposition from sulphate bath, Electrochim. Acta 56 (2011) 7885– 7889.

[8] K. O. Nayana, T. V. Venkatesha, Synergistic effects of additives on morphology, texture and discharge mechanism of zinc during electrodeposition, J. Electroanal. Chem. 663 (2011) 98–107.

[9] L. N. Bengoa, S. Bruno, H. A. Lazzarino, P. R. Seré, W. A. Egli, Study of dendritic growth of zinc crystals on the edges of steel sheet, J. Appl. Electrochem. 44 (2014) 1261–1269.

[10] T. N. Ostanina, V. M. Rudoi, A. V. Patrushev, A. B. Darintseva, A. S. Farlenkov, Modelling the dynamic growth of copper and zinc dendritic deposits under the galvanostatic electrolysis conditions, J. Electroanal. Chem. 750 (2015) 9–18.

[11] R. Y. Wang, D. W. Kirk, G. X. Zhang, Effects of deposition conditions on the morphology of zinc deposits from alkaline zincate solutions, J. Electrochem. Soc. 153 (2006) C357–C364.

[12] P. Pei, K. Wang, Z. Ma, Technologies for extending zinc–air battery's cyclelife: A review, Appl. Energy 128 (2014) 315–324.

[13] S. J. Banik, R. Akolkar, Suppressing Dendritic Growth during Alkaline Zinc Electrodeposition using Polyethylenimine Additive, Electrochim. Acta 179 (2015) 475–481.

[14] D. Desai, X. Wei, D. A. Steingart, S. Banerjee, Electrodeposition of preferentially oriented zinc for flow-assisted alkaline batteries, J. Power Sources 256 (2014) 145–152.

[15] H. -I. Kim, H. -C. Shin, SnO additive for dendritic growth suppression of electrolytic zinc, J. Alloys Compd. 645 (2015) 7–10.

[16] M. Xu, D.G. Ivey, W. Qu, Z. Xie, Study of the mechanism for electrodeposition of dendrite-free zinc in an alkaline electrolyte modified with 1-ethyl-3-methylimidazolium dicyanamide, J. Power Sources 274 (2015) 1249–1253.

[17] D -T. Chin, R. Sethi, J. McBreen, Zinc Electrode Morphology in Alkaline Solutions I. Study of Alternating Voltage Modulation on a Rotating Disk Electrode, J. Electrochem. Soc. 129 (1982) 2677–2685.

[18] M. F. de Carvalho, E. P. Barbano, I. A. Carlos, Influence of disodium ethylenediaminetetraacetate on zinc electrodeposition process and on the morphology, chemical composition and structure of the electrodeposits, Electrochim. Acta 109 (2013) 798–808.

[19] M. F. de Carvalho, I. A. Carlos, Zinc electrodeposition from alkaline solution containing trisodium nitrilotriacetic added, Electrochim. Acta 113 (2013) 229–239.

[20] K. I. Popov, S. S. Djokić, N. D. Nikolić, V. D. Jović, Morphology of Electrochemically and Chemically Deposited Metals. Springer, New York, (2016).

[21] R. Winand, Electrodeposition of metals and alloys – new results and perspectives, Electrochim. Acta 39 (1994) 1091–1105.

[22] A. Gavrilović-Wohlmuther, A. Laskos, Ch. Zelger, B. Gollas, A. Harding Whitehead, Effects of Electrolyte Concentration, Temperature, Flow Velocity and Current Density on Zn Deposit Morphology, Journal of Energy and Power Engineering 9 (2015) 1019–1028.

[23] K. I. Popov, D. N. Keča, M. D. Anđelić, Electrodeposition of Zinc on Copper from Alkaline Zincate Solutions, J. Appl. Electrochem. 8 (1978) 19–23.

[24] Kh. Saber, C. C. Koch, P. S. Fedkiw, Pulse current electrodeposition of nanocrystalline zinc, Mater. Sci. Eng. A 341 (2003) 174–181.

[25] A. Gomes, M. I. da Silva Pereira, Pulsed electrodeposition of Zn in the presence of surfactants, Electrochim. Acta 51 (2006) 1342–1350.

[26] T. Frade, V. Bouzon, A. Gomes, M. I. da Silva Pereira, Pulsed-reverse current electrodeposition of Zn and Zn-TiO2 nanocomposite films, Surf. Coat. Technol. 204 (2010) 3592–3598.

[27] N. P. Wasekar, A. Jyothirmayi, N. Hebalkar, G. Sundararajan, Influence of pulsed current on the aqueous corrosion resistance of electrodeposited zinc, Surf. Coat. Technol. 272 (2015) 373–379.

[28] N. D. Nikolić, Z. Rakočević, K. I. Popov, Reflection and structural analyses of mirror bright metal coatings, J. Solid State Electrochem. 8 (2004) 526–531.

[29] N. D. Nikolić, G. Novaković, Z. Rakočević, D. R. Djurović, K.I. Popov, Comparative reflection and structural analyses of copper and zinc coatings electrodeposited from acid sulfate solutions without and with additives, Surf. Coat. Technol. 161 (2002) 188–194.

[30] R. D. Naybour, Morphologies of zinc electrodeposited from zinc-saturated aqueous alkaline solution, Electrochim. Acta 13 (1968) 763–769.

[31] I. N. Justinijanović, A. R. Despić, Some observations on the properties of zinc electrodeposited from alkaline zincate solutions, Electrochim. Acta 18 (1973) 709–717.

[32] K. I. Popov, N. V. Krstajić, The Mechanism of Spongy Electrodeposits Formation on Inert Substrate at Low Overpotentials, J. Appl. Electrochem. 13 (1983) 775–782.

[33] K. I. Popov, N. V. Krstajić, M. I. Čekerevac, The mechanism of formation of coarse and disperse electrodeposits, in: R.E. White, B.E. Conway, J.O' M. Bockris (Eds.), Modern Aspects of Electrochemistry, vol. 30, Plenum Press, New York, 1996, p.p. 261–312.

[34] J. W. Diggle, A. R. Despić, J. O'M. Bockris, The mechanism of the dendritic electrocrystallization of zinc, J. Electrochem. Soc. 116 (1969) 1503–1514.

[35] J. McBreen, Zinc Electrode Shape Change in Secondary Cells, J. Electrochem. Soc. 119 (1972) 1620–1628.

[36] K. W. Choi, D. N. Bennion, J. Newman, Engineering Analysis of Shape Change in Zinc Secondary Electrodes. I . Theoretical, J. Electrochem. Soc. 123 (1976) 1616–1627.

[37] K. W. Choi, D. Hamby, D. N. Bennion, J. Newman, Engineering Analysis of Shape Change in Zinc Secondary Electrodes. II . Experimental, J. Electrochem. Soc. 123 (1976) 1628–1637.

[38] K. Wang, P. Pei, Z. Ma, H. Xu, P. Li, X. Wang, Morphology control of zinc regeneration for zinc–air fuel cell and battery, J. Power Sources 271 (2014) 65–75.

[39] K. I. Popov, P. M. Živković, B. Jokić, N. D. Nikolić, The shape of the polarization curve and diagnostic criteria for the metal electrodeposition process control, J. Serb. Chem. Soc. 81 (2016) 291–306.

[40] J. O'M. Bockris, Z. Nagy, A. Damjanović, On the Deposition and Dissolution of Zinc in Alkaline Solutions, J. Electrochem. Soc. 119 (1972) 285–295.

[41] K. J. Vetter, Electrochemical Kinetics. Theoretical and Experimental Aspects, Academic Press, New York, 1967.

[42] V. G. Levich, Physicochemical Hydrodynamics, Prentice – Hall, Inc: Englewood Cliffs, Ch. 2, NJ, 1962.

[43] N. D. Nikolić, K. I. Popov, P. M. Živković, G. Branković, A new insight into the mechanism of lead electrodeposition: ohmic–diffusion control of the electrodeposition process, J. Electroanal. Chem. 691 (2013) 66–76.

[44] N. D. Nikolić, K. I. Popov, Lj. J. Pavlović, M. G. Pavlović, Determination of critical conditions for the formation of electrodeposited copper structures suitable for electrodes in electrochemical devices, Sensors 7 (2007) 1–15.

[45] K. I. Popov, P. M. Živković, B. N. Grgur, Physical and mathematical models of an inert macroelectrode modified with active hemispherical microelectrodes, Electrochim. Acta 52 (2007) 4696–4707.

[46] N. D. Nikolić, P. M. Živković, B. Jokić, M. G. Pavlović, J. S. Stevanović, Comparative analysis of the polarisation and morphological characteristics of electrochemically produced powder forms of the intermediate metals, Maced. J. Chem. Chem. Eng. 33 (2014) 169–180.

[47] N. D. Nikolić, K. I. Popov, E. R. Ivanović, G. Branković, S. I. Stevanović, P. M. Živković, The potentiostatic current transients and the role of local diffusion fields in formation of the 2D lead dendrites from the concentrated electrolyte, J. Electroanal. Chem. 739 (2015) 137–148.

[48] K. I. Popov, N. D. Nikolić, General Theory of Disperse Metal Electrodeposits Formation, in: S.S. Djokić (Ed.), Electrochemical Production of Metal Powders, Series: Modern Aspects of Electrochemistry, vol. 54, Springer, 2012, p.p. 1–62.

[49] G. Wranglen, Dendrites and growth layers in the electrocrystallization of metals, Electrochim. Acta 2 (1960) 130–146.

[50] J. S. Newman, Electrochemical Systems, Prentice-Hall, Inc. Engelwood Cliffs, N. J., (1973).

[51] A. R. Despić, K. I. Popov, Transport controlled deposition and dissolution of metals, in: B.E. Conway, J.O' M. Bockris (Eds.), Modern Aspects of Electrochemistry, vol. 7, Plenum Press, New York, 1972, p.p. 199–313.

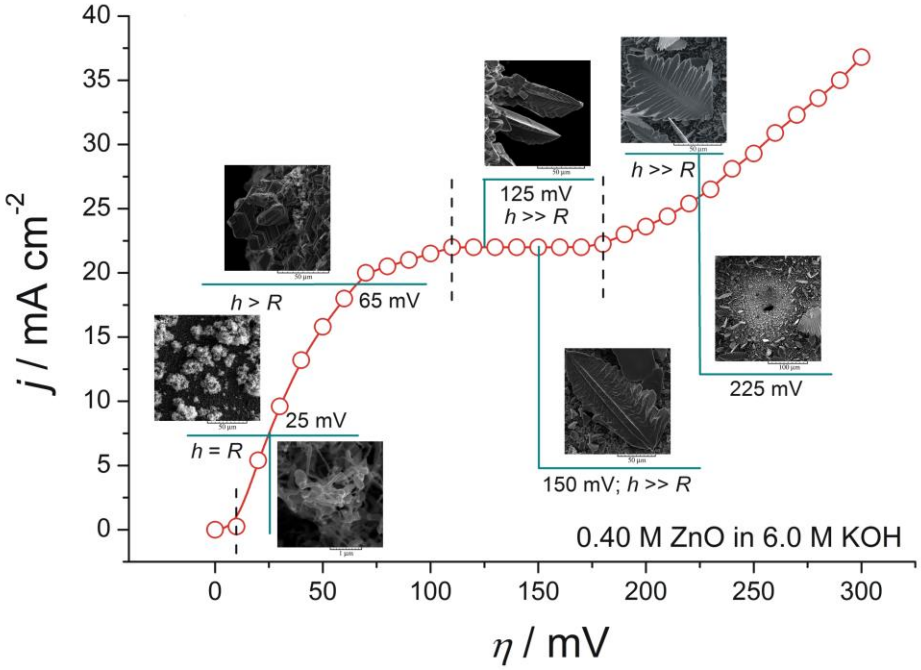

Graphical abstract

Research highlights

- Zinc is electrodeposited potentiostatically from the zincate electrolytes.
- The polarization characteristics of Zn were correlated with the surface morphology.
- The exchange current density for Zn was estimated in the range 18.4–88 mA cm^{-2}.
- A new insight in mechanism of Zn electrodeposition is presented.
- The general theory of disperse deposits formation is used to obtain a new insight.